

## A general template-based method for the preparation of nanomaterials

John C. Hulteen and Charles R. Martin\*†

Department of Chemistry, Colorado State University, Fort Collins, CO 80523, USA

This article reviews a general template-based approach for the preparation of nanomaterials. The method involves the synthesis of a desired material within the pores of a nanoporous membrane. We have termed this approach 'template synthesis' because the pores within these nanoporous membranes act as templates for the synthesis of nanostructures of the desired material. Because the pores within these membranes are cylindrical and of uniform diameter, monodisperse nanocylinders of the desired material are obtained. Depending on the chemistry of the pore wall and material, these nanocylinders may be either hollow (a tubule) or solid (a fibril or nanowire). This template process will be shown to be a very general approach in the fabrication of nanotubes and fibrils composed of a variety of materials including polymers, metals, semiconductors, carbons, and other materials.

### Introduction

Many methods for the fabrication of nanoparticles have been developed, ranging from lithographic techniques to chemical methods.<sup>1,2</sup> This research group has been exploring a fabrication method termed template synthesis for the preparation of a variety of micro- and nano-materials.<sup>3–30</sup> This process involves synthesizing a desired material within the pores of a porous membrane. Because the membranes that are used have cylindrical pores of uniform diameter, a nanocylinder of the desired material is obtained in each pore. Depending on the properties of the material and the chemistry of the pore wall, this nanocylinder may be solid (a nanofibril) or hollow (a nanotubule).

There are a variety of interesting and useful characteristics associated with template synthesis. Probably the most useful feature of this method is that it is extremely general with regard to the types of materials that can be prepared. For example, we have used this method to prepare both nanotubules and nanofibrils composed of conductive polymers,<sup>4–13</sup> metals,<sup>14–25</sup> semiconductors,<sup>26,27</sup> carbon<sup>28–30</sup> and other materials. Next, both tubular and fibrillar nanostructures with very small diameters can be prepared. For example, conductive polymer nanowires with diameters as small as 3 nm have been prepared using this method.<sup>31</sup> Also, because the membranes employed contain cylindrical pores of uniform diameter, monodisperse nanocylinders of the desired material, whose dimensions can be carefully controlled, are obtained. Finally, these tubular or fibrillar nanostructures can be assembled into a variety of architectures. The nanostructures can remain inside the pores of the template membrane or they can be freed from the template membrane and collected as an ensemble of free nanoparticles. Alternatively, if the nanostructure-containing membrane is attached to a surface and the membrane is removed, an ensemble of micro- or nano-structures that protrude from the surface like the bristles of a brush can be obtained.

The intent of this article is to provide an overview of the template method. We will start with a brief description of the types of membranes used for template synthesis. Next, the different types of chemistries that have been used to prepare template-synthesized nanostructures will be reviewed. Finally, we will discuss fundamental properties and applications of template-synthesized metal and semiconductor nanostructures.

While there has been a significant amount of research in the area of template synthesis of conductive polymer nanostructures, this has been reviewed elsewhere recently.<sup>32,33</sup>

### Membranes used

Most of the work in template synthesis, to date, has entailed the use of two types of nanoporous membranes, 'track-etch' polymeric membranes and porous alumina membranes. However, there are a variety of other templates that could be utilized.

#### Track-etch

A number of companies (such as Nucleopore and Poretics) sell microporous and nanoporous polymeric filtration membranes that have been prepared by the track-etch method.<sup>34</sup> This method entails bombarding a non-porous sheet of the desired material (standard thickness range from 6 to 20 mm) with nuclear fission fragments to create damage tracks in the material, and then chemically etching these tracks into pores. The resulting membranes contain randomly distributed cylindrical pores of uniform diameter, Fig. 1(A,B). The commercial membranes are available with pore diameters as small as 10 nm (pore density *ca.*  $10^9$  pores  $\text{cm}^{-2}$ ). These commercial membranes are prepared from polycarbonate or polyester; however, a number of other materials are also amenable to the track-etch process.<sup>34</sup>

Owing to the random nature of the pore-production process, the angle of the pores with respect to the surface normal can be as large as  $34^\circ$ .<sup>35</sup> Therefore, depending on the specific pore diameter and pore density of the track-etched membrane, a number of pores may actually intersect within the membrane. This is a problem when theoretically modelling the optical properties of template-synthesized nanometals, a topic of great interest to our group.<sup>18–20</sup> For example, theory predicts a specific wavelength maximum in the absorption band of isolated metal nanoparticles.<sup>18–20</sup> However, physical contact between the metal nanoparticles synthesized within the pores can shift this absorption maximum by 200 nm or more.<sup>36</sup>

#### Porous alumina

Porous alumina membranes are prepared *via* the anodization of aluminium metal in an acidic solution.<sup>37</sup> These membranes contain cylindrical pores of uniform diameter arranged in a hexagonal array, Fig. 1(C,D). However, unlike the track-etch

† E-mail: crmartin@lamar.colostate.edu

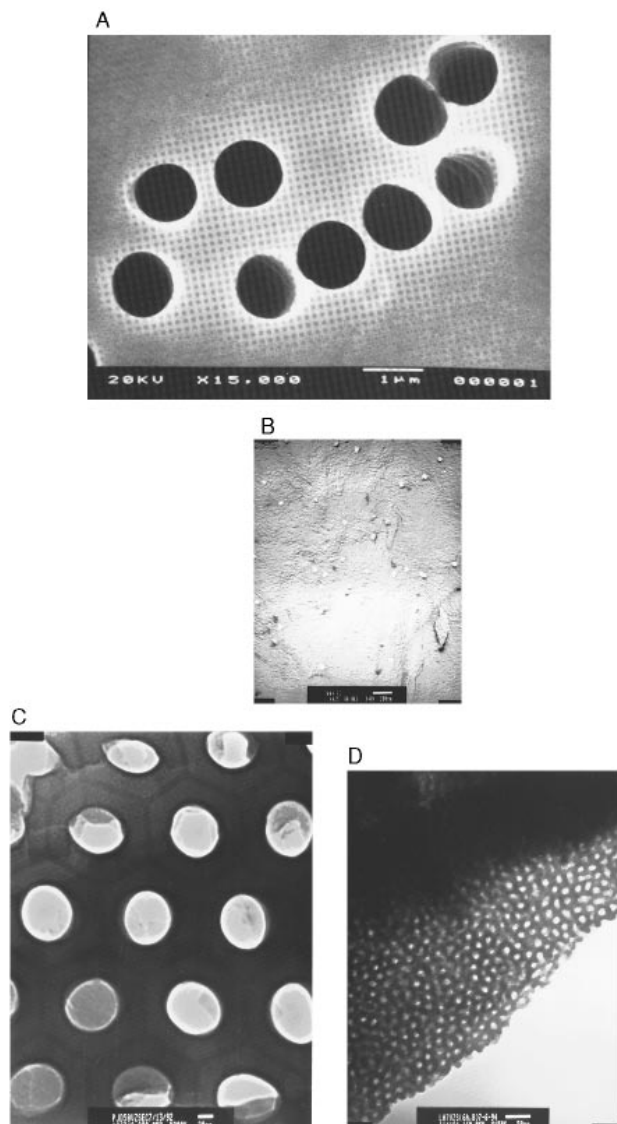


**Fig. 1** Electron micrographs of polycarbonate (A and B) and alumina (C and D) template membranes. For each type of membrane an image of a larger pore membrane is presented (A and C) so that the characteristics of the pores can be clearly seen. Images of a membrane with extremely small pores are also presented (B and D). A, SEM of the surface of a polycarbonate membrane with 1  $\mu\text{m}$  diameter pores. B, TEM of a graphite replica of the surface of a polycarbonate membrane with 30 nm diameter pores. The pores appear 'ragged' owing to the artifact of using a graphite replica. C and D, TEMs of microtomed sections of alumina membranes with 70 nm (C) and 10 nm (D) diameter pores.

membranes, the pores in these membranes have little or no tilt with respect to the surface normal resulting in an isolating, non-connecting pore structure. Although such membranes are sold commercially (Whatman), a very limited number of pore diameters are available. We have, however, prepared membranes of this type with a broad range of pore diameters.<sup>18,20</sup> We have made membranes with pore diameters as large as 200 nm and as small as 5 nm, and we believe that even smaller pores can be prepared. Pore densities as high as  $10^{11}$  pores  $\text{cm}^{-2}$  can be achieved,<sup>38</sup> and typical membrane thickness can range from 10 to 100  $\mu\text{m}$ . The higher pore density is important if one wanted to mass-produce a nanomaterial by the template method. Membranes with high pore density would allow a greater number of nanostructures to be produced per unit area of template membrane.

## Other nanoporous materials

Tonucci *et al.* have recently described a nanochannel array glass with pore diameters as small as 33 nm and pore densities as high as  $3 \times 10^{10}$  pores  $\text{cm}^{-2}$ .<sup>39</sup> Beck *et al.* have prepared a new class of mesoporous zeolites with large pore diameters.<sup>40</sup> Douglas *et al.* have shown that the nanoscopic pores in a protein derived from a bacterium can be used to transfer an image of these pores to an underlying substrate.<sup>41</sup> Clark and Ghadiri have prepared arrays of polypeptide tubules.<sup>42</sup> Finally, both Ozin<sup>1</sup> and Schollhorn<sup>43</sup> have discussed a wide variety of nanoporous solids that could be used as template materials.

## Template synthetic strategies

The limits to which materials can be used in template synthesis are defined by the chemistry required to synthesize the material. Nearly any material can in principle be synthesized within these nanoporous membranes, provided a suitable chemical pathway can be developed. Typical concerns that need to be addressed when developing new template synthetic methods include the following: (1) will the precursor solutions used to prepare the material 'wet' the pore (*i.e.*, hydrophobic/hydrophilic considerations); (2) will the deposition reaction proceed too fast resulting in pore blockage at the membrane surface before tubule/fibre growth can occur within the pores; (3) will the host membrane be stable (*i.e.*, thermally and chemically) with respect to the reaction conditions? The following is a general outline of five representative chemical strategies that have been used in our laboratory to conduct template synthesis within the alumina and polymeric template membranes.

### Electrochemical deposition

Electrochemical deposition of a material within the pores is accomplished by coating one face of the membrane with a metal film (usually *via* either ion sputtering or thermal evaporation) and using this metal film as a cathode for electroplating.<sup>17–22,44,45</sup> This method has been used to prepare a variety of metal nanowires including copper, platinum, gold, silver, and nickel in both track-etch and alumina templates. Typical gold nanowires are shown in Fig. 2(A). The lengths of these nanowires can be controlled by varying the amount of metal deposited. By depositing a small amount of metal, short wires can be obtained; alternatively, by depositing large quantities of metal, long needle-like wires can be prepared.<sup>18–20</sup> This ability to control the length or aspect ratio (length to diameter) of the metal nanowires is especially important in our optical investigations because the optical properties of nanometals are dependent on the aspect ratio.<sup>18–20,24</sup>

Hollow metal tubules can also be prepared *via* this method, Fig. 2(B).<sup>17,22</sup> To obtain tubules, one must typically chemically derivatize the pore walls so that the electrodeposited metal preferentially deposits on the pore wall; that is, a molecular anchor must be applied. For example, gold tubules have been prepared by attaching a cyanosilane to the walls of the alumina template membrane prior to metal depositions.<sup>17,22,46</sup> Owing to the large number of commercially available silanes, this method can provide a general route for tailoring the pore walls in the alumina membranes.

Electrochemical deposition can also be used to synthesize conductive polymers [such as polypyrrole, polyaniline, or poly(3-methylthiophene)] within the pores of these template membranes.<sup>10,13</sup> When these polymers are synthesized within the pores of track-etched polycarbonate membranes, the polymer preferentially nucleates and grows on the pore walls, resulting in polymeric tubules at short polymerization times, Fig. 2(C). By controlling the polymerization time, we can produce thin-walled tubules, thick-walled tubules or solid fibrils.

The reason why the polymer preferentially nucleates and

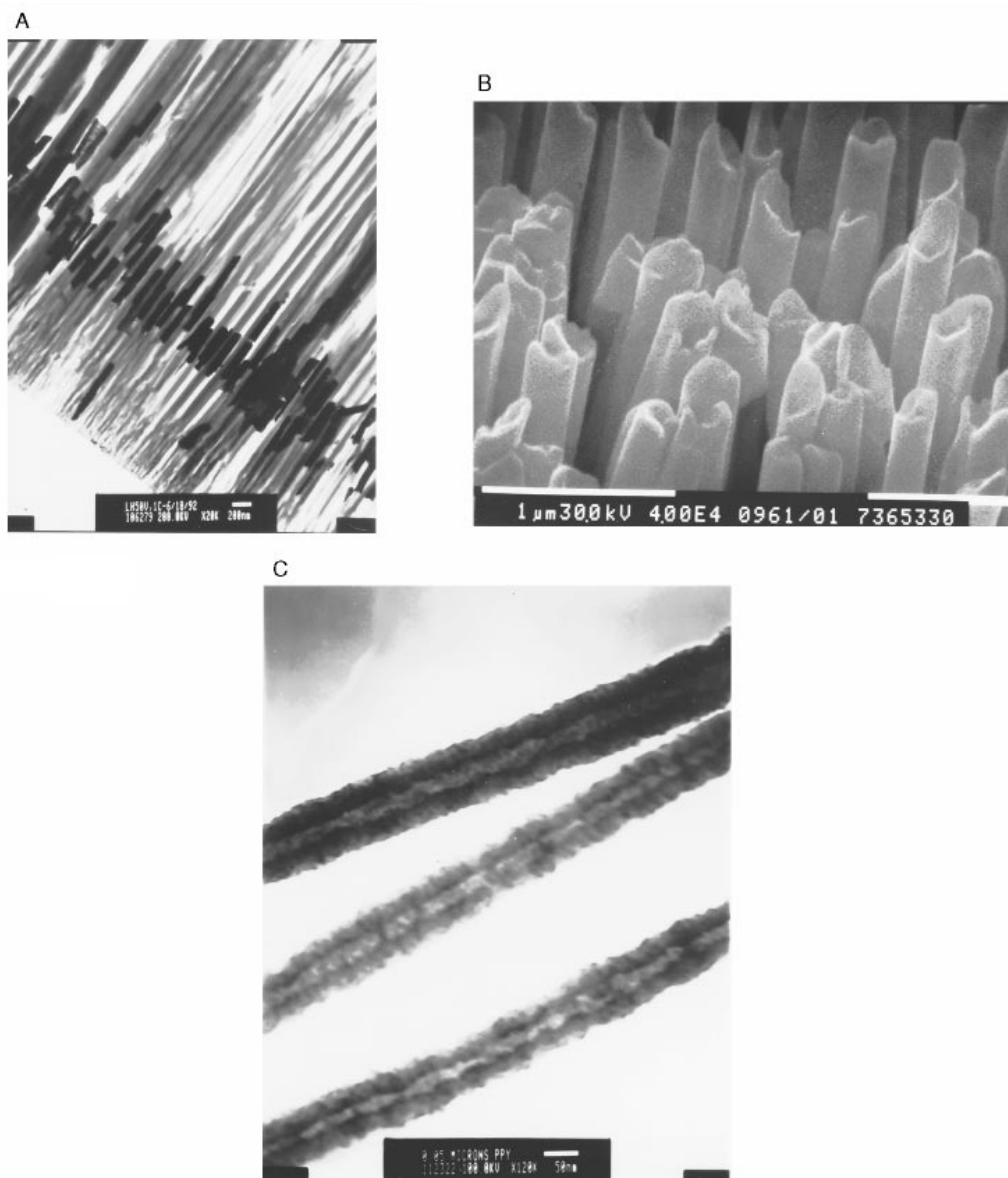


**Fig. 2** Electron micrographs of tubules and fibrils. A, TEM of a microtomed section of an alumina template membrane showing Au nanofibrils that are 70 nm in diameter within the pores. B, SEM of an array of Au microtubules. C, TEM of three polypyrrole nanotubules. The outer diameter is *ca.* 90 nm; the inner diameter is *ca.* 20–30 nm.

grows on the pore walls is straightforward.<sup>8</sup> Although the monomers are soluble, the polycationic forms of these polymers are completely insoluble. Hence, there is a solvophobic component to the interaction between the polymer and the pore wall. There is also an electrostatic component because the polymers are cationic and there are anionic sites on the pore walls.<sup>8</sup>

#### Electroless deposition

Electroless metal deposition involves the use of a chemical reducing agent to plate a metal from solution onto a surface.<sup>47</sup> This method differs from electrochemical deposition in that the surface to be coated need not be electronically conductive. We have developed methods by which gold and other metals can be plated from solution onto the surfaces of both the plastic and alumina membranes.<sup>15</sup> This method involves applying a sensitizer (typically  $\text{Sn}^{2+}$ ) to the membrane surfaces (pore walls and faces). The sensitizer binds to the surfaces *via* complexation with surface amine, carbonyl, and hydroxy groups. This sensitized membrane is then activated by exposure to  $\text{Ag}^+$  resulting in the formation of discrete nanoscopic Ag particles on the membrane's surfaces. Finally, the Ag-coated

membrane is immersed into a Au plating bath containing  $\text{Au}^{\text{I}}$  and a reducing agent, which results in Au plating on the membrane faces and pore walls.

The key feature of the electroless deposition process is that metal deposition in the pores starts at the pore wall. Therefore, after short deposition times, a hollow metal tubule (Fig. 3) is obtained within each pore while long deposition times result in solid metal nanowires. Unlike the electrochemical deposition method where the length of the metal nanowire can be controlled at will, electroless deposition yields structures that run the complete thickness of the template membrane. However, the inside diameter of the tubules formed *via* electroless deposition can be controlled at will by varying the metal deposition time.<sup>15,16</sup> Of course the outside diameter is determined by the diameter of the pores in the template membrane.

#### Chemical polymerization

Chemical template synthesis of a polymer can be accomplished by simply immersing the membrane into a solution containing the desired monomer and a polymerization reagent. This process has been used to synthesize a variety of conductive

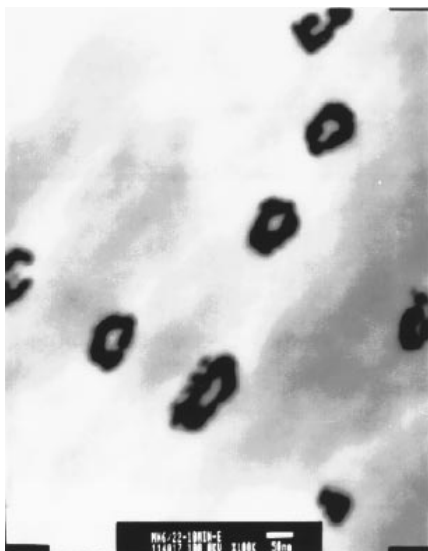


**Fig. 3** TEM showing a microtomed section of a Au nanotubule-containing membrane. The Au tubules are the black rings. The elliptical appearance is caused by the microtoming process. Pore diameter 50 nm; plating time 10 min.

polymers within the pores of various template membranes.<sup>6,9,48,49</sup> As with electrochemical polymerization, the polymer preferentially nucleates and grows on the pore walls, resulting in tubules at short deposition times and fibres at long times.

Conventional (electronically insulating) plastics can also be chemically synthesized within the pores of these template membranes. For example, polyacrylonitrile tubules can be prepared by immersing an alumina template membrane into a solution containing acrylonitrile and a polymerization initiator.<sup>28,29</sup> The inside diameter of the resulting polyacrylonitrile (PAN) tubules is varied by controlling the time the membrane remains in the polymerization bath. These PAN tubules have been further processed to create conducting graphitic carbon tubules and fibrils in alumina membranes, Fig. 4.<sup>28,29</sup> This is accomplished by heating the PAN tubules–alumina membrane composite to 700 °C under an argon flow or under vacuum.

#### Sol–gel deposition

Sol–gel chemistry typically involves hydrolysis of a solution of a precursor molecule to obtain first a suspension of colloidal particles (the sol) and then a gel composed of aggregated sol particles. The gel is then thermally treated to yield the desired product. We have recently conducted various sol–gel syntheses within the pores of the alumina membranes to create both tubules and fibres of a variety of inorganic semiconducting materials including TiO<sub>2</sub>, ZnO and WO<sub>3</sub>.<sup>26</sup> First, an alumina template membrane is immersed into a sol for a given period of time, and the sol deposits on the pore walls. After thermal treatment, either a tubule or fibril of the desired semiconductor is formed within the pores, Fig. 5. As with other template synthesis techniques, longer immersion times yield fibres while brief immersion times produce tubules.

The formation of tubules after short immersion times indicates that the sol particles adsorb to the alumina membrane's pore walls. This is expected because the pore walls are negatively charged while the sol particles used to date<sup>26</sup> are positively charged (a similar situation to what was described for conductive polymers). It has also been found that the rate of gelation is faster within the pore than in bulk solution.<sup>26</sup> This is most likely due to the enhancement in the local concentration of the sol particles due to adsorption on the pore walls.

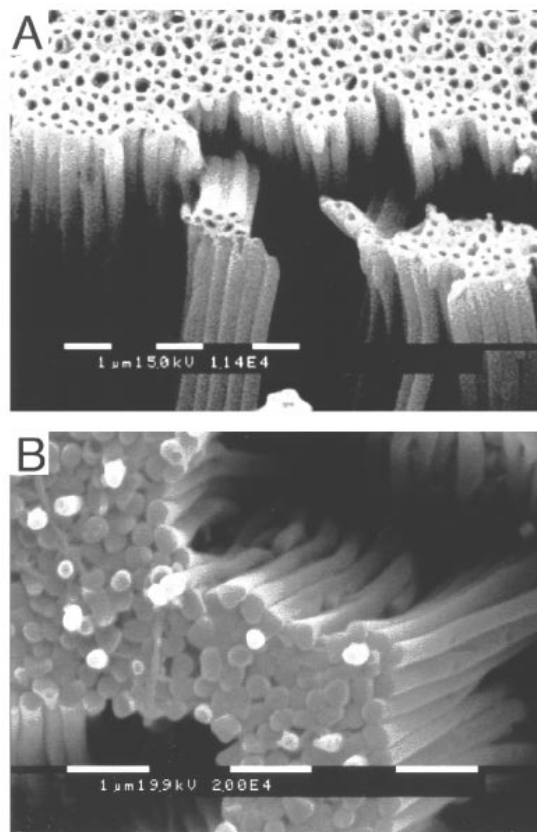


**Fig. 4** SEM images of carbon tubules (A) and fibrils (B) with an outer diameter of 200 nm prepared in an alumina template membrane; membrane was removed for imaging purposes

#### Chemical vapour deposition

A major hurdle in applying chemical vapour deposition (CVD) techniques to template synthesis has been that deposition rates are often too fast. As a result, the surface of the pores becomes blocked before the chemical vapour can traverse the length of the pore. We have, however, developed two template-based CVD syntheses that circumvent this problem. The first entails the CVD of carbon within porous alumina membranes which has been achieved by our group<sup>30</sup> and others.<sup>50</sup> This involves placing an alumina membrane in a high-temperature furnace (*ca.* 700 °C) and passing a gas such as ethene or propene through the membrane. Thermal decomposition of the gas occurs throughout the pores, resulting in the deposition of carbon films along the length of the pore walls (*i.e.*, carbon tubules are obtained within the pores). The thickness of the walls of the carbon tubes is again dependent on total reaction time and precursor pressure.

The second CVD technique utilizes a template-synthesized structure as a substrate for CVD deposition.<sup>51</sup> For example, we have used a CVD method to coat an ensemble of gold nanotubules with concentric TiS<sub>2</sub> outer nanotubules. The first step of this process requires the electroless plating of Au tubules or fibrils into the pores of a template membrane. The Au surface layer is removed from one face of the plated membrane, and the membrane is dissolved away. The resulting structure is an ensemble of Au tubules or fibrils protruding from the remaining Au surface layer like the bristles of a brush, Fig. 6(A). This structure is exposed to the precursor gases used to carry out the CVD synthesis of TiS<sub>2</sub>. As indicated in Fig. 6(B) the Au tubules become coated with outer TiS<sub>2</sub> tubules.

#### Composite nanostructures

We have shown that a large number of different chemical techniques can be used to prepare tubules or fibrils that are

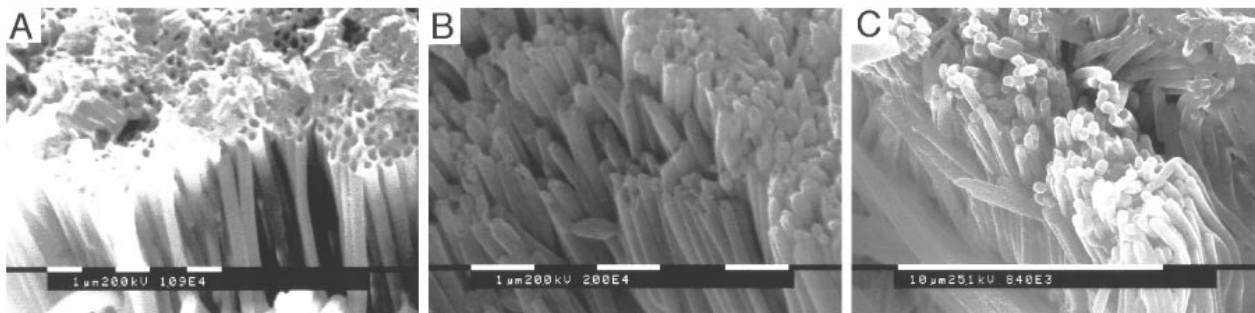


**Fig. 5** SEM images of  $\text{TiO}_2$  tubules and fibrils prepared in an alumina membrane with 200 nm diameter pores. The sol was maintained at  $15^\circ\text{C}$ , and the immersion time varied from 5 to 60 s. A, Immersion time = 5 s; remnants of the  $\text{TiO}_2$  surface layer can be seen in this image. B, Immersion time = 25 s. C, Immersion time = 60 s.

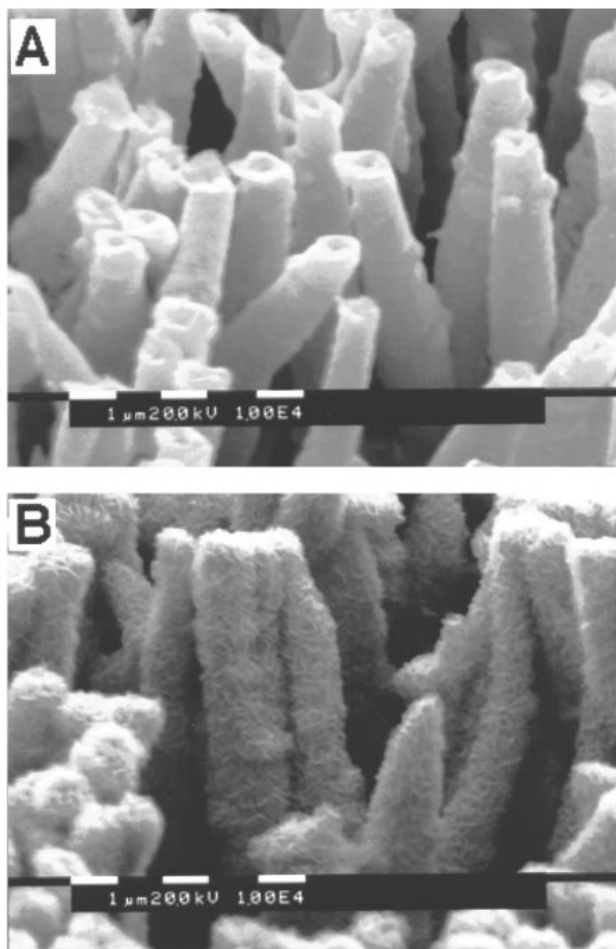


**Fig. 6** SEM images of an ensemble of Au tubules before (A) and after (B) CV deposition of the outer  $\text{TiS}_2$  tubules. The tubules are protruding from the substrate Au surface layer.

composed of a single material. However, one can imagine a host of applications where composite tubular nanostructures would be necessary. Examples might include concentric nanocapacitor or nanobattery tubules. We have recently developed chemical strategies for preparing such concentric tubular nanostructures.<sup>51</sup> These composites have very high interfacial surface areas between concentric layers of materials. High interfacial areas are obtained because the interfaces are parallel to the long axis of the composite tubular nanostructure.

The fabrication of a semiconductor-conductor tubular nano-composite will introduce this concept of sequential tubular synthesis.<sup>51</sup> This composite was prepared in a 60  $\mu\text{m}$  thick alumina template membrane with 200 nm diameter pores. First,  $\text{TiO}_2$  tubules are synthesized within the pores of the

alumina membrane *via* the sol-gel process discussed above, Fig. 7(A). After thermal treatment of the  $\text{TiO}_2$  tubules, conductive polypyrrole nanowires were grown using the chemical polymerization method inside the semiconductor tubules, Fig. 7(B).

$\text{TiO}_2$  is a promising material for photoelectrochemical energy production, and it has been shown that high surface area  $\text{TiO}_2$  has a higher photoefficiency.<sup>52</sup> Therefore, these  $\text{TiO}_2$ -polypyrrole nanocomposites should be excellent photocatalysts because these template-synthesized structures have very high surface area. One problem in using high surface area  $\text{TiO}_2$  as a photocatalyst is the low electrical conductivity of the material. However, this tubular nanocomposite structure should solve this problem because each  $\text{TiO}_2$  tubule has its own current-collecting electrode inside.

Another method for the construction of a two-component

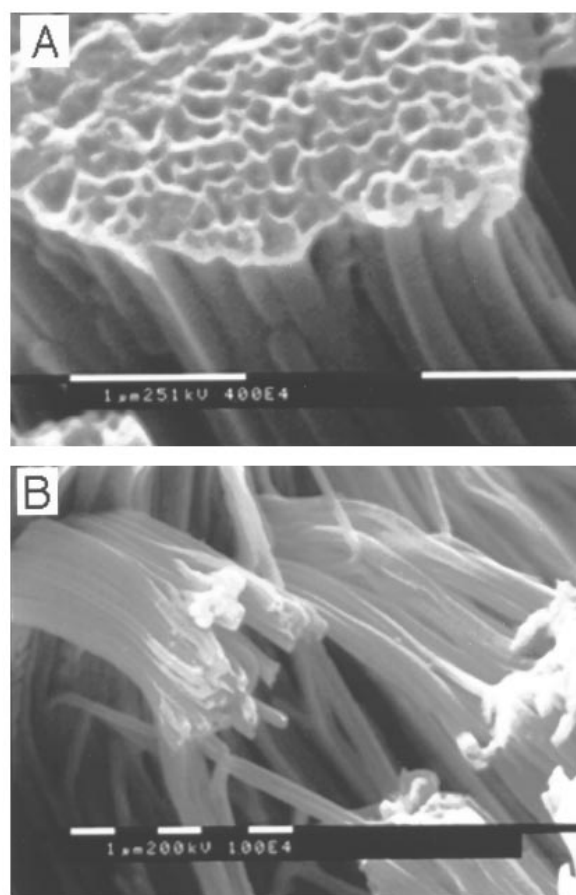


**Fig. 7** SEM images of  $\text{TiO}_2$  nanotubules prepared by sol-gel methods before (A) and after (B) filling with the polypyrrole nanowires. Outer diameter of tubular composite is 200 nm.

concentric composite has already been described, Fig. 6.<sup>51</sup> Gold tubules are electrolessly synthesized within the template membrane pores. The membrane is dissolved away, and a thin film of  $\text{TiS}_2$  is synthesized on the surface of the Au tubules *via* CVD.  $\text{TiS}_2$  is a  $\text{Li}^+$ -intercalation material for Li-based rechargeable batteries. We have recently shown that template-synthesized  $\text{Li}^+$ -intercalating materials can provide higher discharge capacities than conventional electrodes made from the same material.<sup>53</sup> As with the photoconductor materials, many  $\text{Li}^+$ -intercalation materials have low electrical conductivities. However, the current-collecting Au electrode inside each  $\text{TiS}_2$  tubule should again solve this problem. We have shown that the  $\text{TiS}_2$ -polypyrrole composite nanostructures reversibly intercalate and deintercalate  $\text{Li}^+$ , and we are currently investigating the charge-discharge kinetics and capacities of these tubular composite battery electrode materials.

An alternative set of chemistries was used to fabricate a conductor-insulator-conductor composite consisting of carbon-polyacrylonitrile-gold concentric tubules, Fig. 8.<sup>51</sup> Initially, polyacrylonitrile (PAN) tubules were chemically polymerized within the pores of an alumina membrane followed by thermal carbonization resulting in conductive carbon tubules, Fig. 8(B). The PAN polymerization step was then repeated creating insulating PAN tubules within the carbon tubules, Fig. 8(C). A gold film was then sputtered onto one face of the membrane. Using this film, Au nanowires were electroplated within the inner PAN tubules resulting in the desired concentric tubular C-PAN-Au composite structures, Fig. 8(D). We are currently using this synthetic strategy and others to prepare ensembles of nanocapacitors, where all of

the capacitors are connected in parallel from the surfaces of the template membrane. This will require that all of the electronically conductive outer tubules are electronically insulated from the conductive inner nanowires.

Finally, self-assembly chemistry<sup>54</sup> can also be used as a synthetic step to prepare tubular composites. For example, Au tubules were synthesized within the 1  $\mu\text{m}$  pores of a polycarbonate template membrane *via* the electroless deposition method. The inside diameter of these tubules was *ca.* 500 nm, and the length of the tubules was 1.0  $\mu\text{m}$ . The Au tubule-containing membrane was then immersed in a solution of hexadecyl thiol causing the thiol to self-assemble onto the inner surfaces of the Au tubules. The template membrane was dissolved away and the freed tubules were collected by filtration.

When these gold-thiol tubules were placed in water, they floated at the air/water interface owing to the presence of the hydrophobic thiol on the inside of the tubule. In contrast, tubules that were not treated with the thiol filled with water and sank.<sup>51</sup> Because self-assembly provides a general way to apply a large number of different chemical functionalities to the inner (and outer) surfaces of such tubules, composite tubules with diverse inner and outer chemistries should be possible.

These have been just a few examples of the types of composite structures that can be fabricated with template synthesis. Composites composed of a variety of different conducting, insulating, semiconducting, photoconducting and electroactive materials have been prepared. The limits as to how many different components each composite can contain is limited

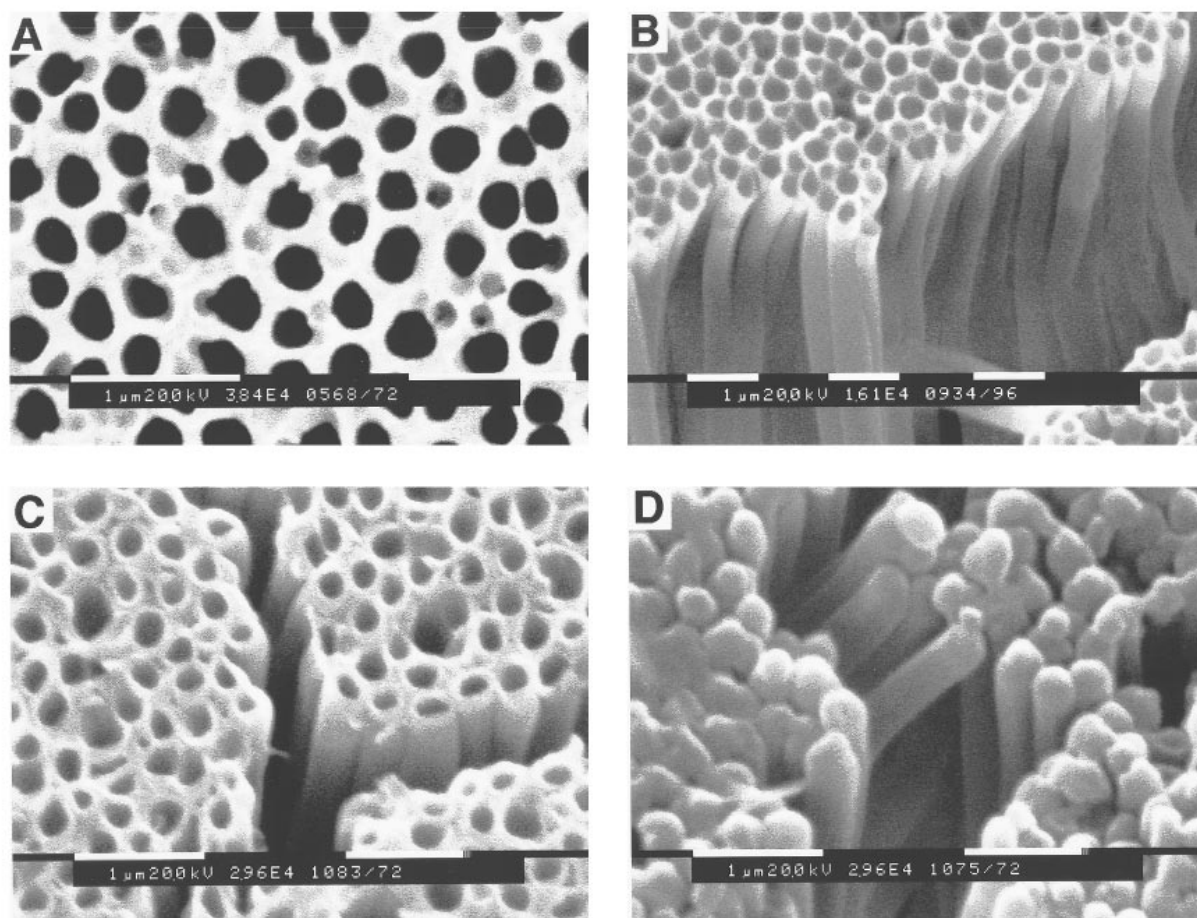


**Fig. 8** A, SEM image of the surface of the alumina template membrane. B, The carbon tubules obtained after dissolution of the template membrane; C, as per B but after polymerization of a PAN tubule within each carbon tubule. D, After electrodeposition of a Au nanowire within each PAN tubule. As noted, the carbon-PAN-Au composites were prepared by performing the appropriate chemistries in sequence leaving the alumina membrane intact; however, it is easier to image these extremely small structures by dissolving the membrane.

only by the initial diameter of the template pore and the rate of material deposition.

### Optical properties of gold nanoparticles

We<sup>18–20</sup> and others<sup>38,55</sup> have been investigating the properties of nanometals prepared within the pores of alumina membranes. Through confinement of metals to a nano-sized dimension, a variety of changes occur in the optical,<sup>18–20,55</sup> electronic<sup>56</sup> and magnetic<sup>38,57</sup> properties. The first demonstration of template synthesis for the creation of nanometal fibrils was by Possin in 1970.<sup>58</sup> Earlier work in which nanometals were used to colour alumina is also of interest.<sup>59</sup> Nanometal-containing membranes of this type have also been used as selective solar absorbers.<sup>60</sup> Finally, magnetic metals have been deposited within the pores of such membranes to make vertical magnetic recording media.<sup>61</sup>

This research group<sup>18–20</sup> and others<sup>55</sup> have been primarily interested in the fundamental optical properties of nanocylinders of Au imbedded into alumina membranes. The colours of colloidal suspensions of Au can range from red to purple to blue depending on the diameter of the particles,<sup>62</sup> and we have been able to demonstrate analogous colours for Au particles electroplated into the alumina template membrane.<sup>18–20</sup> These colours result from shape-induced changes in the plasmon resonance band of the Au nanoparticle which corresponds to the wavelength of light that induces the largest electric field on the nanoparticles.

### Fabrication

The gold nanoparticles are prepared using the electrodeposition method discussed above, Fig. 9.<sup>18–20</sup> First, Ag is deposited onto one face of an alumina template membrane to provide a conductive film for electrodeposition, Fig. 9(A). The membrane is placed, Ag film side down, on a glass plate and covered with a Ag plating solution. Then, short Ag 'plugs' or 'posts' are electrochemically grown into the pores, Fig. 9(B). These Ag nanoposts are used as foundations onto which the Au nanoparticles are electrochemically grown, Fig. 9(C). Finally, the Ag foundations are removed with a nitric acid wash resulting in an array of Au nanoparticles imbedded within the pores of the alumina membrane, Fig. 9(D).

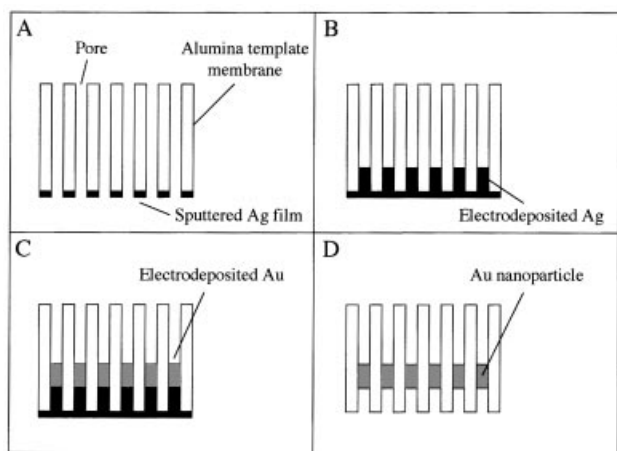


**Fig. 9** Fabrication procedure for Au nanoparticle–alumina composite. A, Ag is sputtered on one side of the host alumina membrane. B, Membrane is placed sputtered side down onto a glass plate, and a Ag foundation is deposited electrochemically. C, Au is electrochemically deposited onto the Ag foundations. D, Ag is removed with nitric acid.

### Structural characterization

The diameter of the electroplated gold nanoparticles is equivalent to the pore diameter of the alumina template membrane. Thus, Au nanoparticles with different diameters can be fabricated in alumina membranes containing different pore diameters. The aspect ratio is controlled by changing the amount of Au electrochemically deposited into the pores. However, we have found that it is not possible to quantitatively predict the aspect ratio of the Au nanoparticles because the plating current efficiency varies from membrane to membrane.<sup>24</sup> Hence, it is not possible to calculate the aspect ratio of the Au nanoparticle obtained from the known quantity of Au deposited and the pore diameter and density. Therefore, transmission electron microscopy (TEM) analysis of the Au nanoparticles synthesized in each membrane is necessary to determine the lengths (and aspect ratios) of the nanoparticles.<sup>24</sup> A TEM image of a transverse section of a Au nanoparticle–alumina composite is shown in Fig. 2(A). When different amounts of Au are electrodeposited within the pores of the template membrane, we can produce Au nanoparticle shapes that are prolate, spheroid or oblate.<sup>24</sup>

### Optical characterization

The differences in the shapes of the Au nanoparticles result in changes in the optical absorption properties of the composite.<sup>18–20,24</sup> Such changes are clearly visible as a membrane's colour can vary from a bright red to deep blue to turquoise depending on the particle shape.<sup>18–20,24</sup> The alumina membranes are optically transparent, so the colours are predominantly due to the Au nanoparticles. It should also be noted that the parallel orientation of the pores in the alumina membrane confines the Au particles to a single dimensional alignment. Correspondingly, there is no ambiguity in particle orientation which is a necessary feature for theoretical modelling of the absorption spectrum.

Fig. 10 shows the experimental absorption spectra for a variety of Au nanoparticle–alumina composites. The Au particle aspect ratio (length/diameter) varies from 7.7 to 0.38, and

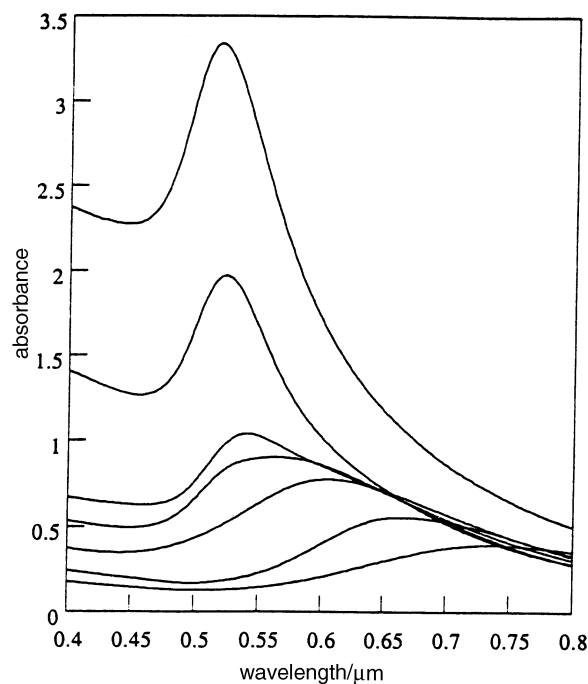


**Fig. 10** Experimental absorption spectra for the Au nanoparticle containing membranes. The spectrum with the highest absorbance maximum is for the membrane containing the aspect ratio (length/diameter) of 7.7, followed by 2.7, 1.3, 0.77, 0.54, 0.46 and 0.38 respectively.



the diameter of each Au particle is constant at *ca.* 52 nm. The reduction in absorption intensity with decreasing aspect ratio is expected due to the decrease in the metal volume fraction of the composites. The shift in the absorption maximum from 518 nm (aspect ratio 7.7) to 738 nm (aspect ratio 0.38) is predicted from simulated spectra obtained using a dynamic Maxwell-Garnett theory.<sup>24</sup>

This article shows that the template method can be used to fabricate Au nanoparticles with various diameters and aspect ratios. Shifts in the absorption maximum and changes in the absorption intensity of the Au nanoparticle-alumina composites have been studied as a function of both particle diameter and aspect ratio. Current work involves determining the effects of heating the Au nanoparticle-alumina composite. Changes in the Au nanoparticles aspect ratios, optical properties and crystal structure have been observed.

## Nanoelectrode ensembles

One very exciting application of template synthesis is in the area of electrochemistry. Nanoelectrodes offer opportunities to perform electrochemistry in highly resistive media<sup>63,64</sup> and to investigate the kinetics of redox processes that are too fast to measure at conventional macroscopic electrodes.<sup>65-68</sup> (By macroscopic electrodes we mean disk-shaped electrodes with diameters of the order of 1 mm.) We have used the template method to prepare ensembles of Au nanodisk electrodes where the diameters of the Au disks are as small as 10 nm.

### Fabrication

Using the electroless Au deposition procedure, Au nanowires are synthesized within the pores of a polycarbonate track-etch membrane. In addition, both faces of the membrane become coated with thin Au films. If one of these surface Au films is removed, the disk-shaped ends of the Au nanowires traversing the membrane are exposed. These nanodisks can be used as active elements in an ensemble of nanoelectrodes. Fig. 11 shows a schematic of such a nanoelectrode ensemble (NEE).<sup>14</sup> Electrical contact is made to the remaining surface layer which acts as a common current collector for all the nanoelectrode elements.

A consistent problem associated with micro- and nanoelectrodes is achieving an efficient seal between the conductive element and the host material. If a good seal is not achieved, solution can creep into this junction resulting in significantly

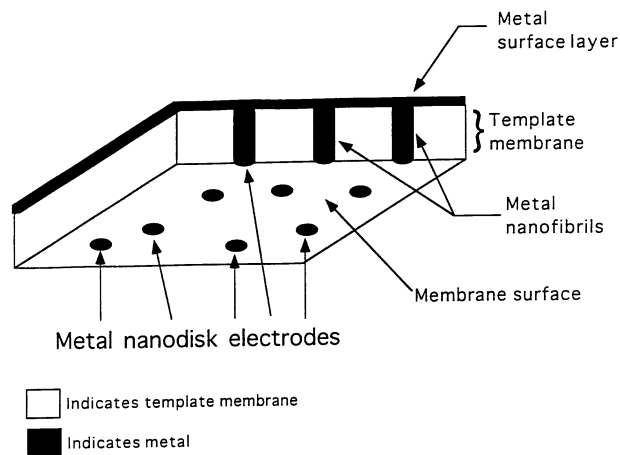


**Fig. 11** Schematic of an edge view of a nanoelectrode ensemble. The nanometal fibrils running through the pores of the template membrane are shown. The lower ends of the fibrils define nanodisks which are the electrodes. The opposite (upper) ends of the nanofibrils are connected to a common metal film which is used to make electrical contact to the nanodisks.

higher values of the background or double-layer charging currents. In the case of the NEE, the polycarbonate is stretch-oriented during fabrication to improve mechanical properties. Upon heating above the glass transition temperature (*ca.* 150 °C), the membrane relaxes, shrinks, and seals the junction between the Au nanowires and the polymer membrane.<sup>14,15</sup>

### Current response of the NEE

Two different electrochemical response limiting cases can be observed at an NEE, the 'total overlap' and 'radial' response.<sup>14</sup> Which limiting case is achieved depends strongly upon the distance between the electrode elements and the timescale (*e.g.*, scan rate) of the electrochemical experiment. When the electrode elements are in close proximity and the scan rate is relatively low, the diffusion layers at each electrode element overlap, Fig. 12(A). This overlap results in a single diffusion layer that covers the total geometric area of the NEE. Linear diffusion occurs to the entire NEE surface, and conventional peak-shaped voltammograms are obtained. Also, the total faradaic current is equivalent to that obtained at an electrode of equivalent geometric area whose entire surface area is gold.

If the electrode elements are located far apart and the timescale of the experiment is relatively fast, the diffusion layers at each electrode element act independently resulting in a radial diffusion field at each individual electrode element, Fig. 12(B). The voltammogram in this case has a sigmoidal shape, and the predicted total faradaic current is equivalent to the sum of the current generated at each individual electrode element within the NEE.

Fig. 13 shows a series of SEM images of NEEs with varying average distances between the electrode elements.<sup>14</sup> The NEEs were fabricated from polymer template membranes with different pore densities but similar pore diameters. Fig. 14 presents the faradaic response of an electroactive species [trimethylaminomethylferrocene (TMAFc<sup>+</sup>)] at each of these NEEs.<sup>14</sup> The NEE with the highest electrode element density [Fig. 13(A), Fig. 14(A)] shows a peak-shaped voltammogram indicative of the total overlap response. In contrast, the NEE with the lowest electrode element density [Fig. 13(D), Fig. 14(D)] shows the expected sigmoidal voltammogram. The other two NEEs have an intermediate nanoelectrode density [Fig. 13(B,C), Fig. 14(B,C)] and show an intermediate response.

We can demonstrate quantitatively that the NEEs in Fig. 13(A,D) are operating in the total overlap and radial

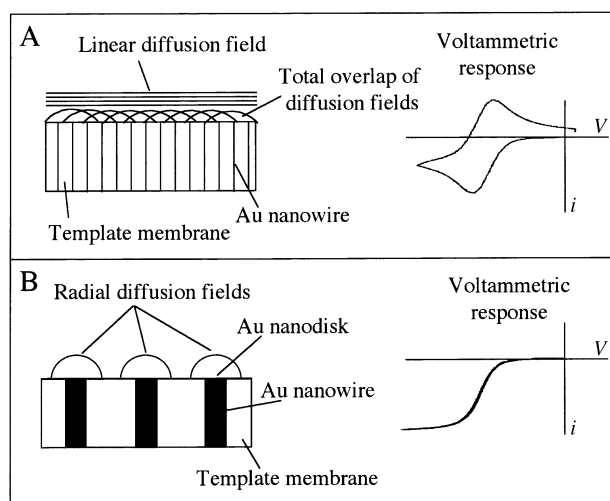


**Fig. 12** Schematic of a side view of NEEs and the corresponding diffusion fields for the total overlap (A) and radial (B) limiting electrochemical response



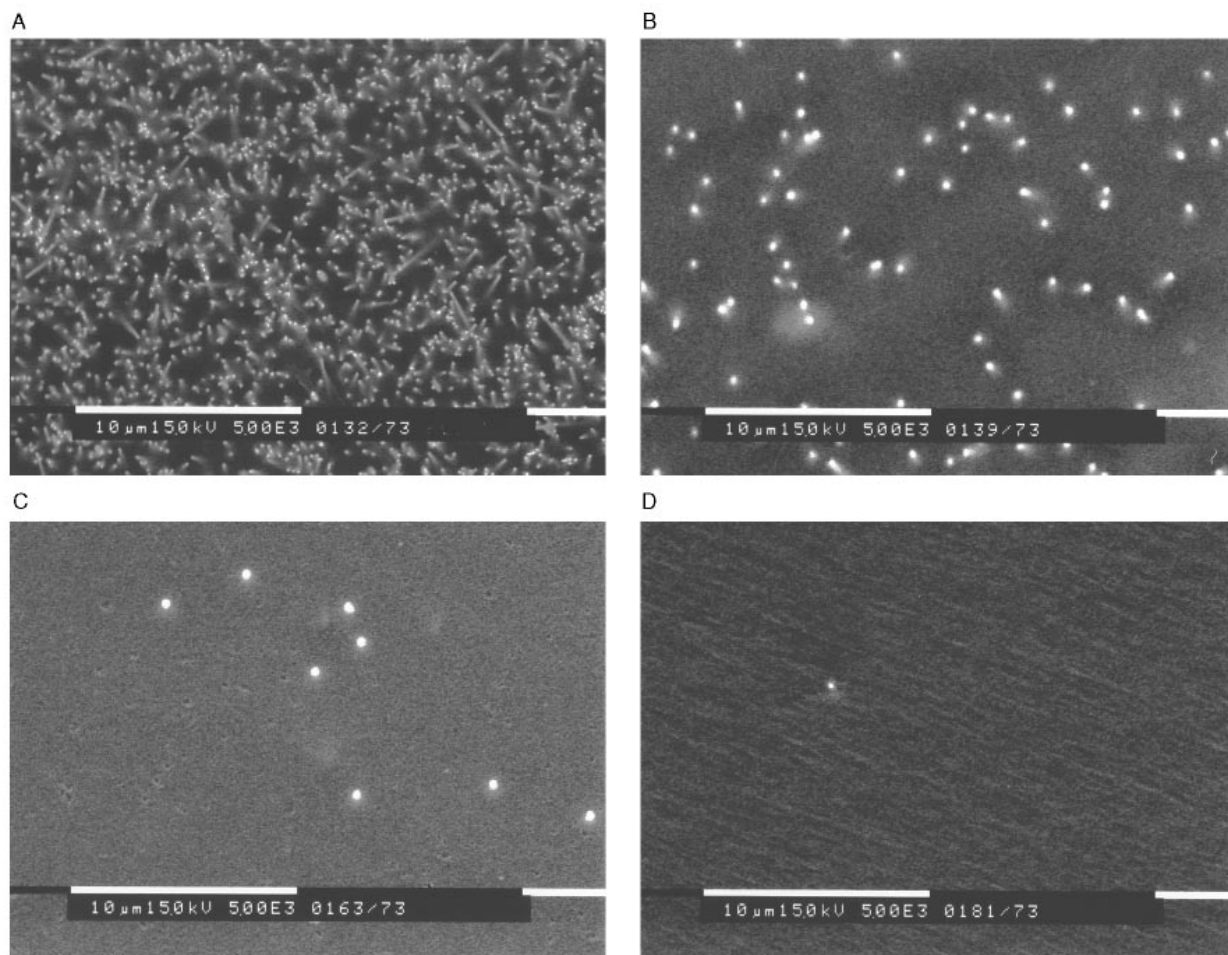


**Fig. 13** SEM images of the surfaces of NEEs showing the disk-like electrode elements prepared from membranes with varying pore densities. Average distance between pores are: A, 0.25 mm; B, 1.1 mm; C, 3.5 mm; D, 17.5 mm. Diameters of electrode elements are 100 nm (A,D) and 200 nm (B,C).

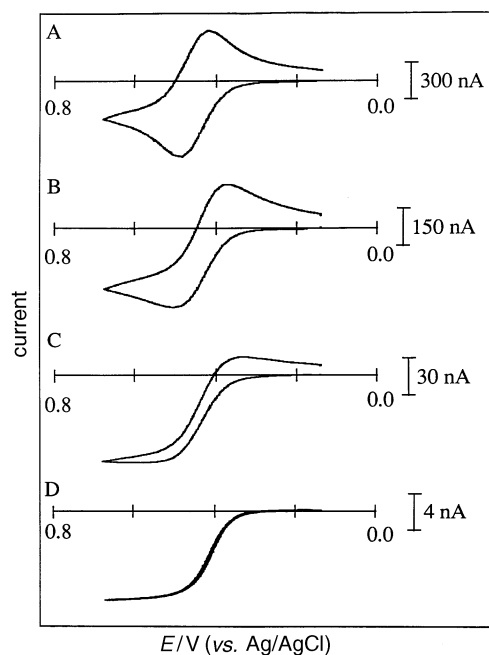


**Fig. 14** Cyclic voltammograms ( $50 \text{ mV s}^{-1}$ ) for 50 mM TMAFc<sup>+</sup> in 5 mM NaNO<sub>3</sub> for NEEs prepared from the membranes shown in Fig. 13

response modes by comparing experimental and simulated voltammograms. Such a comparison is shown in Fig. 15. The simulated voltammogram in Fig. 15(A) is based on the reversible total overlap limiting case, and the experimental voltammogram is the same as Fig. 14(A).<sup>14</sup> The quantitative

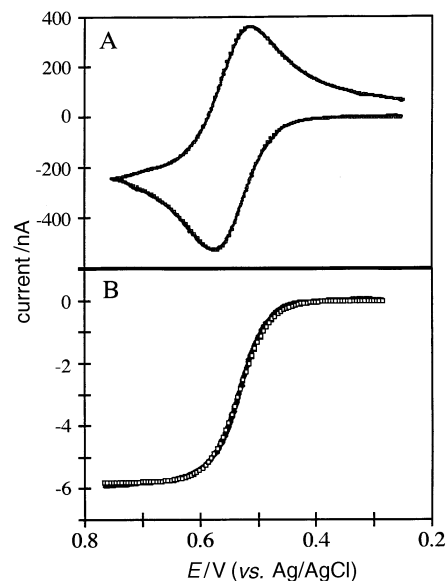


**Fig. 15** Simulated and experimental voltammograms for NEEs prepared from Fig. 13A and D. Scan rate and solution same as Fig. 14.

agreement between the simulated and experimental voltammograms confirms that the NEEs at this pore density and scan rate are in the total overlap electrochemical response. It is important to point out that there are no adjustable parameters in this simulation.

The simulated voltammogram in Fig. 15(B) assumes a single 100 nm diameter disk electrode, but the total current is multiplied by the number of electrodes within the geometric area of the NEE. The experimental voltammogram is equivalent to Fig. 14(D). The quantitative agreement between the simulated and experimental voltammograms proves that the radial electrochemical response has been achieved at this NEE. Again, there are no adjustable parameters in this simulation.

### Detection limits

A possible application of these NEEs is the ultra trace detection of electroactive species. We have recently shown that NEEs with 10 nm diameter disks operating in the total overlap mode show electroanalytical detection limits that are three orders of magnitude lower than detection limits obtained at macroscopic Au disk electrodes of comparable geometric area.<sup>15</sup> This occurs because in the total overlap mode, the total faradaic signal generated at the NEE is equivalent to that obtained at the conventional macroelectrode of equivalent geometric area. However, the background double-layer charging current is significantly less because these currents are proportional only to the active Au area. The ratio of active area to geometric area for a 10 nm NEE is approximately 0.001.<sup>15</sup> As a result, the background current is reduced by three orders of magnitude, and detection limits can be improved by three orders of magnitude.

An example of this enhancement in detection limits at an NEE is shown in Fig. 16.<sup>15</sup> Fig. 16(A) shows voltammograms at a conventional Au macroelectrode at various low concentrations of TMAFc<sup>+</sup>. As expected, the faradaic signal eventually vanishes into the double-layer charging currents as the concentration of TMAFc<sup>+</sup> decreases. Fig. 16(B) shows voltammograms at a NEE with 10 nm diameter electrode

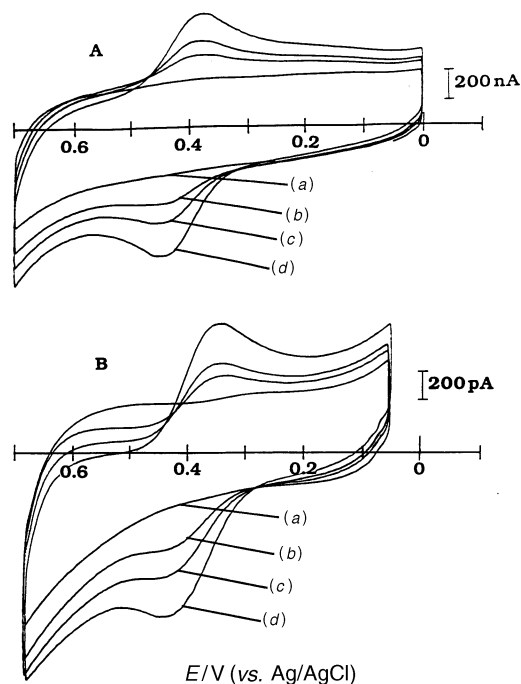


**Fig. 16** Cyclic voltammograms at  $100 \text{ mV s}^{-1}$  in aqueous TMAFc<sup>+</sup> at (A) a gold macrodisk electrode in  $50 \text{ mM NaNO}_3$  [TMAFc<sup>+</sup>] =  $0.5$  (a),  $7.8$  (b),  $15.6$  (c),  $31.2 \text{ } \mu\text{M}$  (d); (B) a  $10 \text{ nm}$  NEE in  $1 \text{ mM NaNO}_3$  [TMAFc<sup>+</sup>] =  $0.5$  (a),  $7.8$  (b),  $15.6$  (c),  $31.2 \text{ nM}$  (d).

elements and a geometric area equivalent to that of the macroelectrode at various low concentrations of TMAFc<sup>+</sup>. While the voltammograms essentially look identical to those obtained at the macroelectrode, the concentrations of the electroactive species at the NEE are three orders of magnitude lower than those for the macroelectrode. The detection limit at the macroelectrode was determined to be *ca.*  $2 \text{ } \mu\text{M}$  while the detection limit at the NEE was *ca.*  $2 \text{ nM}$ .<sup>15</sup>

Template synthesis has been shown to provide a simple means of creating ensembles of nanoelectrode ensembles. These NEEs can achieve electroanalytical detection limits that are three orders of magnitude lower than detection limits obtained at conventional macroelectrodes. We are currently investigating fabrication processes that allow the use of NEEs in non-aqueous solvents.

### Metal nanotube membranes

We close our discussion of metal nanostructures with an interesting new type of membrane consisting of Au nanotubes that span the complete thickness of the membrane. We have previously mentioned that by controlling the electroless Au deposition time, the inside diameters of these tubes can be controlled at will. We recently asked the question, can tubes with inside diameters that approach the sizes of molecules be prepared, and if so, what applications might exist for such nanotubule containing membranes?

### Fabrication

Typical templates used to prepare the metal nanotubule membranes were  $6 \text{ } \mu\text{m}$  thick polycarbonate membranes with  $50 \text{ nm}$  pore diameters and  $6 \times 10^8$  pores  $\text{cm}^{-2}$ . Gold was electrolessly plated onto the walls of the pores yielding a Au nanotube within each pore. Variation in the plating time has been shown to produce Au tubules with internal diameters ranging from  $34$  to  $1.4 \text{ nm}$ .<sup>16</sup> The diameter of these Au tubules was determined from measurements of gas (He) flux across the membrane.<sup>16</sup> Because the electroless process plates on the membrane surface as well as within the pores, electrical contact with the surface allows electrical control of the potential inside the pores.

### Ion-selective membranes

The ion transport properties of these Au nanotubule-containing membranes were studied using a U-tube concentration cell where the membrane separates two differing aqueous solutions, Fig. 17.<sup>16</sup> In an initial experiment, differing concentrations of KCl were placed on each side of the membrane, and reference electrodes were inserted into each solution to measure the membrane potential ( $E_m$ ). When the diameters of the Au nanotubules approached  $2 \text{ nm}$  or less, the membranes dis-

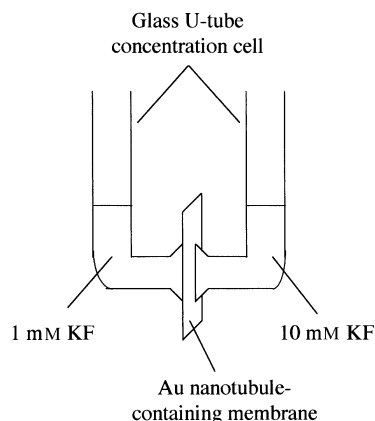


**Fig. 17** Schematic of a U-tube concentration cell

played near ideal cation-permselective behaviour, *i.e.*, these membranes transport cations but reject anions.<sup>16</sup> This behaviour occurs because  $\text{Cl}^-$  adsorbs strongly to Au, and as a result, the Au tubules have an excess of negative charge ( $\text{Cl}^-$ ) on their inner surfaces. This causes anions to be excluded from the pores.

Ion permselectivity can also be controlled by directly changing the potential applied to the Au nanotubules. For this work, it was essential to use an anion that does not adsorb to Au because we wanted to control the charge in the Au tubes and not have it predetermined due to excess charge from counterion adsorption. Because  $\text{F}^-$  does not adsorb to Au, KF was chosen as the electrolyte. The U-tube assembly was used again, but this time the membrane was connected to the working electrode lead of a potentiostat. The potential applied to the Au nanotube membrane varied from  $-0.5$  to  $+0.5$  V *vs.* Ag/AgCl. The membrane was placed between solutions of 10 mM and 1 mM KF, and  $E_m$  values were measured at each applied potential.

The dashed lines at the top and bottom of Fig. 18 are the  $E_m$  values that would be achieved if the nanotubule membrane showed ideal cation and ideal anion permselectivity, respectively. At negative applied potentials, the nanotubule membrane shows ideal cation permselectivity, whereas at positive applied potentials the membrane shows ideal anion permselectivity. This selectivity occurs because at negative applied potentials, an excess negative charge is present on the walls of the Au tubes. This results in the exclusion of anions from the tubes. At positive applied potentials, the opposite situation occurs: cations are excluded and anions are transported.

For any combination of metal and electrolyte, there is a potential called the potential of zero charge (p.z.c.) where there is no excess charge on the metal. At this potential the nanotubule membranes should show neither cation nor anion permselectivity, and  $E_m$  should approach 0 mV.  $E_m$  for the tubule-containing membrane goes from the ideal cation permselective value, through zero, to the ideal anion permselective value. Furthermore, the potential at which  $E_m$  approaches zero is close to the reported p.z.c. ( $-4$  mV).<sup>69</sup>

We have demonstrated that these Au nanotubule-containing membranes can be cation permselective, anion permselective, or non-selective depending on the potential applied to the membrane. These membranes can be as permselective as the commercially available Nafion polymer and should have appli-

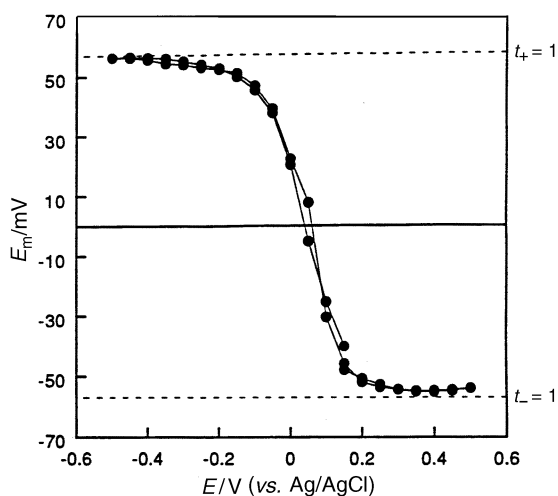


**Fig. 18** Variation of  $E_m$  with potential applied to the membrane [1 mM KF on the low concentration (l) side, and 10 mM KF on the high concentration (h) side of the membrane; tubule radius *ca.* 1.1 nm]. The potential of the membrane was controlled with a potentiostat *vs.* a Ag/AgCl reference electrode immersed in the side-h solution.  $E_m$  was measured with the membrane under potentiostatic control.

cations in both fundamental and applied electrochemistry. Because the Au tubules have dimensions of the order of molecular sizes and are quite monodisperse, we have been exploring the possibility of separating molecules based upon differences in their physical dimensions.

## Semiconductor nanotubules and nanofibres

Electrochemical methods have been used previously as a means of depositing semiconductor materials into the pores of a template membrane.<sup>27</sup> However, this section will discuss the properties of semiconductor tubules and fibrils synthesized by a much more versatile deposition method, sol-gel chemistry.<sup>26</sup>

### Structural characterization

Upon the confinement of a semiconductor to nanoscopic dimensions, the first two questions that arise are: can we see evidence for quantum confinement, and what is the crystal structure of the material?  $\text{TiO}_2$  fibrils have been synthesized within the pores of both 200 nm and 22 nm pore diameter alumina membranes.<sup>26</sup> The sol-gel fabrication of  $\text{TiO}_2$  fibrils within the pores of alumina membranes was described earlier. An absorption spectrum of the template alumina membrane containing these fibres showed an abrupt increase in absorbance at an approximate wavelength of 389 nm. This corresponds to the bandgap of bulk  $\text{TiO}_2$ .<sup>70</sup> This suggests that the diameter of these fibrils is too large to see evidence for quantum confinement in the absorption spectrum. We are capable of preparing alumina template membranes with pore diameters approaching 5 nm or smaller. Correspondingly, we are currently attempting to prepare fibrils small enough to provide evidence for quantum confinement.

Electron diffraction has been employed to determine the crystal structure of the template-synthesized  $\text{TiO}_2$  fibrils.<sup>26</sup> Fig. 19(A) shows a TEM image of 15 nm diameter  $\text{TiO}_2$  nanofibres with the membrane dissolved away. The small fibres are arranged in bundles which can contain anywhere from 2 to 10 or more fibres. Fig. 19(B) shows the indexed electron diffraction pattern obtained from the centre of the fibril bundle on the left side of the main feature in Fig. 19(A). The orientations of the images are the same, *i.e.*, the  $c^*$  axis in Fig. 19(B) is parallel to the fibril bundle axis in Fig. 19(A). These data show that the fibrils are highly crystalline anatase-phase  $\text{TiO}_2$ , with the  $c^*$  axis of the anatase oriented along the long axis of the fibril. Small fibril bundles throughout the sample display the same crystalline orientation; *i.e.*, the reciprocal lattice direction [110] is almost always parallel to the electron beam, and the  $c^*$  axis is along the fibril axis. We have concluded that these fibrils crystallize as long, prismatic crystals with the rare,

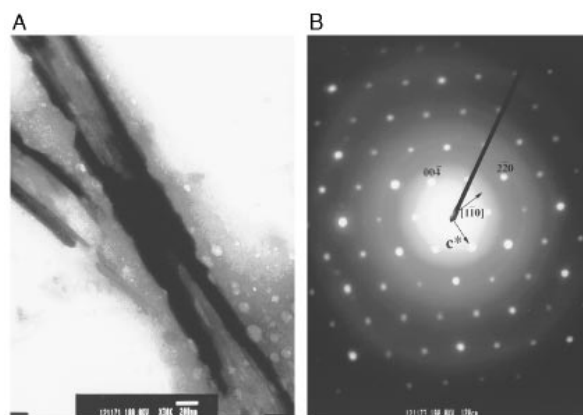


**Fig. 19** A, TEM image of a bundle of 15 nm diameter  $\text{TiO}_2$  fibrils. B, Corresponding electron diffraction pattern.

and metastable, anatase mineralogical orientation [001] with {100}.<sup>71</sup>

### Photocatalysis

A standard application of TiO<sub>2</sub> has been as a photocatalyst for the decomposition of organic molecules.<sup>72–76</sup> This is a surface reaction that is thought to involve absorption of a UV photon by TiO<sub>2</sub> to produce an electron–hole pair which reacts with water to yield hydroxyl and superoxide radicals. These radicals can then oxidize the organic molecule. Template-synthesized TiO<sub>2</sub> structures should increase the TiO<sub>2</sub> surface area and correspondingly increase the decomposition reaction rates. For example, TiO<sub>2</sub> fibrils can be synthesized within the pores of a 60 μm thick alumina membrane with 200 nm diameter pores.<sup>26</sup> The TiO<sub>2</sub> fibril-containing membrane is attached to an epoxy surface, and the membrane is dissolved away. The calculated surface area of the immobilized fibrils is 315 cm<sup>2</sup> of TiO<sub>2</sub> surface area per cm<sup>2</sup> of planar geometric area. This suggests that, in principle, an enhancement of 315 in the catalytic rate of organic decomposition on template-synthesized TiO<sub>2</sub> fibres is possible *versus* a thin film TiO<sub>2</sub> catalyst. Through the use of tubular structures and/or template membranes with smaller diameter pores (with correspondingly higher pore densities and surface area) even larger increases in the rate would be predicted.

We have studied the decomposition of salicylic acid over time on an array of immobilized TiO<sub>2</sub> fibres, Fig. 5(C), with exposure to sunlight, Fig. 20(A).<sup>26</sup> The upper curve follows the concentration of salicylic acid for a solution containing no TiO<sub>2</sub> catalyst, and no significant decomposition is observed. The small increase in salicylic acid concentration has been ascribed to the evaporation of water during the exposure to sunlight. The middle curve follows salicylic acid decomposition on a thin film of TiO<sub>2</sub>, and the bottom curve shows a marked increase in decomposition of salicylic acid for the template-synthesized TiO<sub>2</sub> fibres.

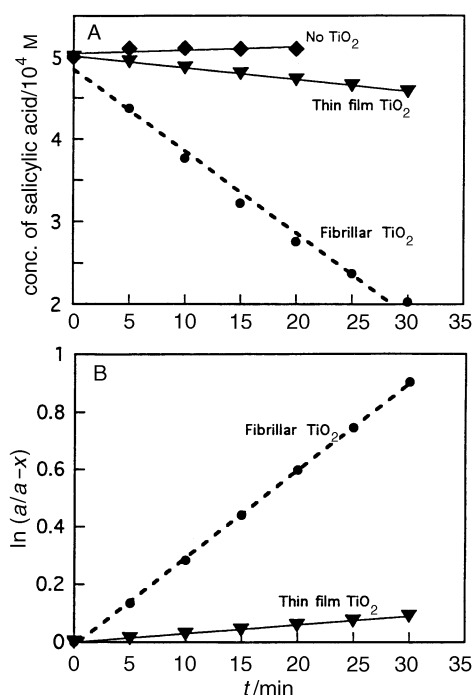


**Fig. 20** A, Photodecomposition of salicylic acid in sunlight. Data for no photocatalyst, the thin film TiO<sub>2</sub> photocatalyst, and the fibrillar (200 nm) TiO<sub>2</sub> photocatalyst are shown. B, First-order kinetics of the photodecomposition of salicylic acid with both the thin film and fibrillar TiO<sub>2</sub> photocatalyst.

The decomposition data can be used to determine quantitatively the rate of photodecomposition. If a pseudo-first-order rate law with respect to the salicylic acid concentration is plotted *versus* reaction time, rate constants for the decomposition of salicylic acid can be determined, Fig. 20(B).<sup>73,75–77</sup> The slope of these lines provides the decomposition rate constant. The thin film catalyst has a rate constant of 0.003 min<sup>-1</sup> while the fibrillar catalyst shows an increased rate constant of 0.03 min<sup>-1</sup>. This order of magnitude increase in reaction rate is much smaller than the 315 times enhancement predicted. This is not surprising because the thin film TiO<sub>2</sub> undoubtedly has some degree of surface roughness resulting in higher surface areas and higher decomposition rates than predicted. Also, scanning electron microscopy (SEM) analysis of the fibrillar TiO<sub>2</sub>, Fig. 5(C), shows that the fibres ‘lean’ against each other, possibly shading large portions of the surface from the sunlight resulting in lower decomposition rates than predicted.

Single-crystal TiO<sub>2</sub> fibrils can be fabricated *via* template synthesis and sol–gel chemistry. Also, owing to the increased surface area of the TiO<sub>2</sub> fibril array, the decomposition rate of an organic molecule increases. However, this prototype fibrillar catalyst is not optimal. We are currently working on processes to optimize the fibril arrays by varying the fibril diameter and aspect ratio and the distance between the fibrils. We are also exploring additional applications of these TiO<sub>2</sub> nanofibres including electrochemistry, battery research, photoelectrochemistry and enzyme immobilization.

### Conclusions

The template method has become a very simple yet powerful process for the synthesis of nanomaterials. This article has described a host of chemistries that are now available for the template synthesis of a wide variety of nanomaterials including metals, polymers, carbon, and semiconductors. Applications have ranged from fundamental optical studies to ultra trace molecular detection to high surface area catalysis.

What does the future hold for template synthesis? From a fundamental viewpoint, our group is interested in fabricating nanostructures with significantly smaller diameters in order to explore further the effects of size on the properties of materials. We are also developing new chemistries so that tubules and fibrils composed of an even larger variety of materials are available. New applications for template-synthesized nanomaterials are also being developed. We are exploring applications in photocatalysis, chemical analysis, bioencapsulation, biosensors, bioreactors, molecular separations, and electronic and electrooptical devices. Finally, it is clear that if practical applications are to be realized, methods for mass producing template-synthesized nanostructures will be required.

This work would not have been possible without the efforts of a number of hardworking and highly motivated graduate students and postdocs. They include Vinod P. Menon, Zhihua Cai, Junting Lei, Wenbin Liang, Ranjani V. Parthasarathy, Charles J. Brumlik, Gabor L. Hornyak, Leon S. Van Dyke, Colby Foss, Matsuhiko Nishizawa, Reginald M. Penner, Charles J. Patrissi, Veronica M. Cepak, Brinda B. Lakshmi, Guangli Che and Kshama B. Jirage. Financial support from the National Science Foundation, the Office of Naval Research and the Department of Energy is also gratefully acknowledged. We also wish to thank the Colorado State University Electron Microscopy Center.

### References

- 1 G. A. Ozin, *Adv. Mater.*, 1992, **4**, 612.
- 2 *Engineering a Small World: From Atomic Manipulation to Microfabrication*, special section of *Science*, 1991, **254**, 1300–1342.

- 3 C. R. Martin, *Chem. Mater.*, 1996, **8**, 1739.
- 4 R. V. Parthasarathy and C. R. Martin, *J. Polym. Sci.*, 1996, **62**, 875.
- 5 C. R. Martin and R. V. Parthasarathy, *Adv. Mater.*, 1995, **7**, 487.
- 6 R. Parthasarathy and C. R. Martin, *Nature (London)*, 1994, **369**, 298.
- 7 C. R. Martin, R. Parthasarathy and V. Menon, *Synth. Met.*, 1993, **55–57**, 1165.
- 8 C. R. Martin, *Adv. Mater.*, 1991, **3**, 457.
- 9 Z. Cai, J. Lei, W. Liang, V. Menon and C. R. Martin, *Chem. Mater.*, 1991, **3**, 960.
- 10 L. S. Van Dyke and C. R. Martin, *Langmuir*, 1990, **6**, 1123.
- 11 W. Liang and C. R. Martin, *J. Am. Chem. Soc.*, 1990, **112**, 9666.
- 12 Z. Cai and C. R. Martin, *J. Am. Chem. Soc.*, 1989, **111**, 4138.
- 13 R. M. Penner and C. R. Martin, *J. Electrochem. Soc.*, 1986, **133**, 2206.
- 14 J. C. Hulteen, V. P. Menon and C. R. Martin, *J. Chem. Soc., Faraday Trans.*, 1996, **92**, 4029.
- 15 V. P. Menon and C. R. Martin, *Anal. Chem.*, 1995, **67**, 1920.
- 16 M. Nishizawa, V. P. Menon and C. R. Martin, *Science*, 1995, **268**, 700.
- 17 C. J. Brumlik, V. P. Menon and C. R. Martin, *J. Mater. Res.*, 1994, **9**, 1174.
- 18 C. A. Foss Jr., G. L. Hornyak, J. A. Stockert and C. R. Martin, *J. Phys. Chem.*, 1994, **98**, 2963.
- 19 C. A. Foss Jr., G. L. Hornyak, J. A. Stockert and C. R. Martin, *Adv. Mater.*, 1993, **5**, 135.
- 20 C. A. Foss Jr., G. L. Hornyak, J. A. Stockert and C. R. Martin, *J. Phys. Chem.*, 1992, **96**, 7497.
- 21 C. J. Brumlik, C. R. Martin and K. Tokuda, *Anal. Chem.*, 1992, **64**, 1201.
- 22 C. J. Brumlik and C. R. Martin, *J. Am. Chem. Soc.*, 1991, **113**, 3174.
- 23 R. M. Penner and C. R. Martin, *Anal. Chem.*, 1987, **59**, 2625.
- 24 G. L. Hornyak and C. R. Martin, *J. Phys. Chem.*, 1997, **101**, 1548.
- 25 G. L. Hornyak, C. J. Patrissi and C. R. Martin, *Thin Solid Films*, submitted.
- 26 B. B. Lakshmi, P. K. Dorhout and C. R. Martin, *Chem. Mater.*, 1997, **9**, 857.
- 27 J. D. Klein, R. D. I. Herrick, D. Palmer, M. J. Sailor, C. J. Brumlik and C. R. Martin, *Chem. Mater.*, 1993, **5**, 902.
- 28 R. V. Parthasarathy, K. L. N. Phani and C. R. Martin, *Adv. Mater.*, 1995, **7**, 896.
- 29 J. C. Hulteen, X. C. Chen and C. R. Martin, in preparation.
- 30 G. Che, K. B. Jirage, E. R. Fisher and C. R. Martin, *J. Electrochem. Soc.*, submitted.
- 31 C.-G. Wu and T. Bein, *Science*, 1994, **264**, 1757.
- 32 C. R. Martin, *Handbook of Conductive Polymers*, in press.
- 33 C. R. Martin, *Acc. Chem. Res.*, 1995, **28**, 61.
- 34 R. L. Fleisher, P. B. Price and R. M. Walker, *Nuclear Tracks in Solids*, University of California Press, Berkeley, CA, 1975.
- 35 Poretics Corporation, Livermore, CA, Product Guide, 1995.
- 36 M. Quinten and U. Kreibitz, *Surf. Sci.*, 1986, **172**, 557.
- 37 A. Despic and V. P. Parkhutik, in *Modern Aspects of Electrochemistry*, ed. J. O'M. Bockris, R. E. White and B. E. Conway, Plenum Press, New York, 1989, vol. 20, ch. 6.
- 38 D. AlMawawi, N. Coombs and M. Moskovits, *J. Appl. Phys.*, 1991, **70**, 4421.
- 39 R. J. Tonucci, B. L. Justus, A. J. Campillo and C. E. Ford, *Science*, 1992, **258**, 783.
- 40 J. S. Beck, J. C. Vartuli, W. J. Roth, M. E. Leonowicz, C. T. Kresge, K. D. Schmitt, C. T.-W. Chu, D. H. Olson, E. W. Sheppard, S. B. McCullen, J. B. Higgins and J. L. Schlenker, *J. Am. Chem. Soc.*, 1992, **114**, 10834.
- 41 K. Douglas, G. Devaud and N. A. Clark, *Science*, 1992, **257**, 642.
- 42 T. D. Clark and M. R. Ghadiri, *J. Am. Chem. Soc.*, 1995, **117**, 12364.
- 43 R. Schollhorn, *Chem. Mater.*, 1996, **8**, 1747.
- 44 S. K. Chakarvarti and J. Vetter, *J. Micromech. Microeng.*, 1993, **3**, 57.
- 45 M. J. Tierney and C. R. Martin, *J. Phys. Chem.*, 1989, **93**, 2878.
- 46 C. J. Miller, C. A. Widrig, D. H. Charych and M. Majda, *J. Phys. Chem.*, 1988, **92**, 1928.
- 47 *Electroless Plating: Fundamentals and Applications*, ed. G. O. Mallory and J. B. Hajdu, American Electroplaters and Surface Finishers Society, Orlando, FL, 1990, ch. 1, pp. 1–55.
- 48 J. Lei, Z. Cai and C. R. Martin, *Synth. Met.*, 1992, **46**, 53.
- 49 R. V. Parthasarathy and C. R. Martin, *Chem. Mater.*, 1994, **6**, 1627.
- 50 T. Kyotani, L. Tsai and A. Tomita, *Chem. Mater.*, 1996, **8**, 2109.
- 51 V. M. Cepak, J. C. Hulteen, G. Che, K. B. Jirage, B. B. Lakshmi, E. R. Fisher and C. R. Martin, *Chem. Mater.*, 1997, **9**, 1065.
- 52 B. O'Regan and M. Grätzel, *Nature (London)*, 1991, **335**, 737.
- 53 M. Nishizawa, K. Muaki, S. Kuwabata and C. R. Martin, *J. Electrochem. Soc.*, in press.
- 54 G. M. Whitesides and J. P. Mathius, *Science*, 1991, **254**, 1312.
- 55 C. K. Preston and M. Moskovits, *J. Phys. Chem.*, 1993, **97**, 8495.
- 56 J. T. Masden and N. Giordino, *Phys. Rev. B*, 1987, **36**, 4197.
- 57 T. M. Whitney, J. S. Jiang, P. C. Searson and C. L. Chien, *Science*, 1993, **261**, 1316.
- 58 G. E. Possin, *Rev. Sci. Instrum.*, 1970, **41**, 772.
- 59 T. Asada, *Jpn. Pat.*, 1960, 310401.
- 60 R. D. Patel, M. G. Takwale, V. K. Nagar and V. G. Bhide, *Thin Solid Films*, 1984, **115**, 169.
- 61 S. Kawai, in *Symposium on Electrochemical Technology in Electronics*, Electrochemical Society, Pennington, NJ, 1987, p. 389.
- 62 J. C. van de Hulst, *Light Scattering by Small Particles*, Dover, New York, 1981, pp. 397–400.
- 63 S. M. Drew and R. M. Wrightman, *J. Electroanal. Chem.*, 1991, **317**, 117.
- 64 M. F. Bento, M. J. Medeiros, M. L. Montenegro, C. Beriot and D. Pletcher, *J. Electroanal. Chem.*, 1993, **345**, 273.
- 65 A. Russell, K. Repka, T. Dibble, J. Ghoroghchian, J. J. Smith, M. Fleischmann, C. H. Pitt and S. Pons, *Anal. Chem.*, 1986, **58**, 2961.
- 66 A. M. Bond, T. L. E. Henderson, D. R. Mann, W. Thormann and C. G. Zoski, *Anal. Chem.*, 1988, **60**, 1878.
- 67 N. Oyama, T. Ohsaka, N. Yamamoto, J. Matsui and O. J. Hatosaki, *J. Electroanal. Chem.*, 1989, **265**, 297.
- 68 Z. J. Karpinski and R. A. Osteryoung, *J. Electroanal. Chem.*, 1993, **349**, 285.
- 69 J. Clavilier and C. N. V. Huong, *J. Electroanal. Chem.*, 1977, **80**, 101.
- 70 B. Enright and D. Fitzmaurice, *J. Phys. Chem.*, 1986, **100**, 1027.
- 71 J. D. Dana (rewritten by C. Polache, H. Berman and C. Frondel), *The System of Mineralogy*, John Wiley, NY, 1955.
- 72 A. Fujishima and K. Honda, *Nature (London)*, 1972, **37**, 238.
- 73 R. W. Matthews, *J. Phys. Chem.*, 1987, **91**, 3328.
- 74 B. Kraeutler and A. J. Bard, *J. Am. Chem. Soc.*, 1978, **100**, 5985.
- 75 D. F. Ollis, C. Hsiao, L. Budiman and C. Lee, *J. Catal.*, 1984, **88**, 89.
- 76 K. Okamoto, Y. Yamamoto, H. Tanaka, M. Tanaka and A. Itaya, *Bull. Chem. Soc. Jpn.*, 1985, **58**, 2015.
- 77 R. W. Mathews, *J. Catal.*, 1987, **97**, 565.

Paper 7/00027H; Received 2nd January, 1997